Separation of kinetic and mass transport effects in the electrolysis of formic acid in a flow-through cell

Qingxin Zhang, Azam Sayadi and Peter G. Pickup*

Department of Chemistry, Memorial University, St. John's, Newfoundland, Canada A1B 3X7

Electrochimica Acta 294 (2019) 110-116

https://doi.org/10.1016/j.electacta.2018.10.088

Abstract

The effects of mass transport and kinetics have been separated by analysis of the flow rate dependence of the current for formic acid oxidation at fuel cell electrodes in a flow-through cell. The mass transport limiting current was reached when a carbon supported Pd catalyst was used, which allowed the power of the flow rate dependence to be determined. Simulation of the flow rate dependence of the current in the mixed kinetic-mass transport region then allowed the electron transfer rate constant and kinetic current to be determined as a function of potential. Comparison of Tafel plots for the Pd electrode and a Pt black electrode demonstrated that the superior activity of Pd was primarily due to its lower Tafel slope. The flow-through cell geometry allows measurements to be made on fuel cell electrodes at high current densities, and provides kinetic parameters that are not influenced by diffusion of the reactant into the catalyst layer.

Keywords: Flow cell; formic acid; electrocatalysis; Tafel; mass transport; kinetics

*Corresponding author. Tel.: +1-709-864-8657; Fax: 1-709-864-3702

E-mail address: ppickup@mun.ca (P.G. Pickup)

1. Introduction

The electrochemical oxidation of organic fuels such as formic acid, methanol and ethanol is of both fundamental and applied importance. Applications include fuel cells [1], electrolysis to produce hydrogen [2, 3], and sensors. Whereas formic acid oxidation is relatively simple, with only a few adsorbed intermediates, and one electrochemical product, methanol and ethanol oxidation involve both adsorbed and desorbed intermediates, and multiple products. Consequently, measurement of the kinetics and stoichiometries of these reactions is challenging.

Studies of the oxidation of organic fuels generally rely heavily on cyclic voltammetry, which provides a wealth of qualitative information, but is difficult to interpret [4] because of the large number of time dependent processes that control the current at any point. These include electrochemical and chemical kinetics, diffusion, the product distribution, and populations of adsorbed and solution intermediates. The time dependence is often measured by chronoamperometry [5], which has been used to quantify the rate of accumulation of adsorbed CO during formic acid oxidation [6]. Rotating disc voltammetry (RDV) has been used to explore the effects of convection, separate the kinetic and mass transport components of the current, and measure stoichiometry [7-9]. However, the validity of using the Kouteky-Levich equation to analyze RDV data for reactions with soluble intermediates (e.g. oxygen reduction, methanol and ethanol oxidation) has been questioned [8, 10], and changes in the populations of adsorbates can produce inaccurate results [8].

Recently, there has been growing interest in the use of flow cells to study the electrochemical characteristics of catalyst materials that are being developed for fuel cells and a variety of other applications [11-14]. This is important because mass transport plays such an important role in these systems. RDV is the standard method for controlling mass transport in

fundamental electrochemical studies, but has some limitations that can more easily be avoided by use of a flow system [15]. Flow systems allow much more flexible cell designs that can accommodate the wide range of materials used in electrochemical technologies [15, 16], can be operated at elevated temperature [17], and allow rapid changing of the electrolyte solution [16, 18] and collection of products [15].

We report here on a simple flow cell that has been designed for kinetic studies on the oxidation of organic fuels at the types of electrodes employed in fuel cells and electrolysis cells. Since these types of cells are normally operated under mixed kinetic and mass transport control, the primary objective was the separation of kinetic and mass transport effects in order to accurately determine kinetic parameters at high current densities. A schematic diagram of the cell is shown in Fig. 1A. A two-electrode, flow-through design, with co-facial electrodes and no reference electrode, was employed in order to minimize the effects of solution resistance and avoid uneven potential and current distributions. During oxidation of a fuel at the anode, an almost constant potential is maintained at the downstream cathode by the evolution of hydrogen. Consequently, the cathode acts as a dynamic hydrogen electrode (DHE). This concept has been employed for many years in fuel cell research [19, 20].

In RDV and conventional thin-layer, channel, and wall-jet flow cells, the reactant diffuses into the catalyst layer through an external diffusion layer, and intermediates and products diffuse out from the same side, as illustrated in Fig. 1B. This can lead to low utilization of the catalyst in thick layers with low permeability. The advantage of the flow-through design employed here is that the reactant and intermediates flow through the whole catalyst layer, maximizing the utilization of the catalyst, and allowing intermediates to react further as they flow through the catalyst layer (Fig. 1C).

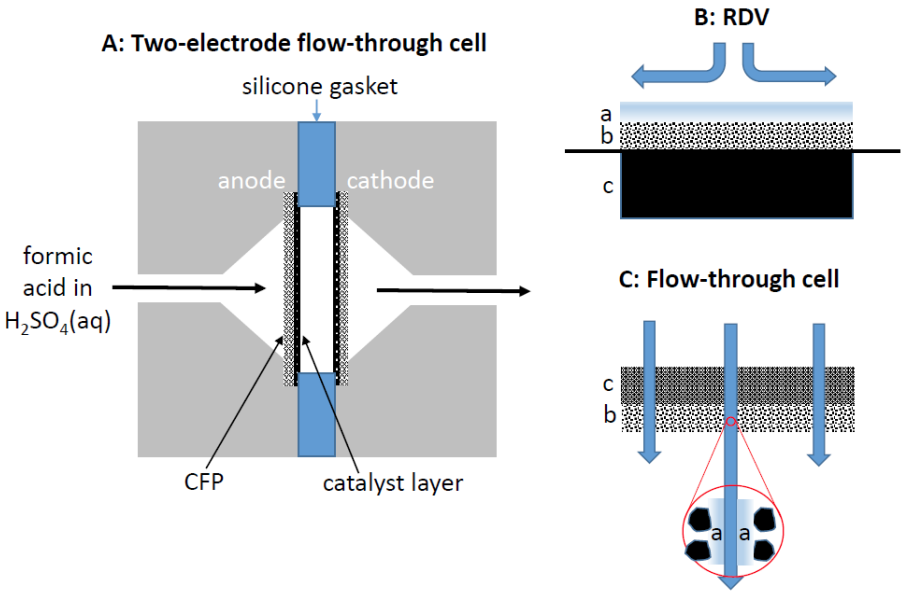

Figure 1. Schematic diagram of the flow-through cell (A), and the solution flow and diffusion layer (a) in rotating disc voltammetry (B) and the flow-through cell employed in this work (C). b is the catalyst layer and c is the support material.

The objectives of this work were to characterize the hydrodynamic characteristics of the cell so that mass transport effects could be assessed, and separated from the effects of electron transfer kinetics. Initially, Fe^{2+} and $Fe(CN)_6^{4-}$ oxidation was investigated in an attempt to measure mass transport limited currents, but these reactions were found to be unsuitable because they occurred on both the catalyst (Pt) and carbon support. Consequently, formic acid oxidation at a carbon supported Pd catalyst (Pd/C) was used to characterize the hydrodynamic behavior of the cell, which was then be used to separate the kinetic and mass transport currents for formic acid at both Pd/C and Pt black electrodes.

2. Experimental

2.1. Materials solutions and electrodes.

Formic acid (Sigma-Aldrich), sulfuric acid (Fisher Scientific), 40% HP Pd on Vulcan XC-72 (Pd/C; E-TEK Division of BASF; average crystallite size of 4.2 nm from X-ray diffraction (4.0 nm specified by E-TEK)), Nafion® solution (5%, Dupont), 1-propanol (Sigma-Aldrich), and carbon fiber paper (CFP; Toray) were used as received. Pt black electrodes (proprietary) consisted of 4 mg Pt cm^{-2} with a PTFE binder on wet-proofed CFP, while the Pd/C electrode was prepared on CFP with 1.05 mg Pd cm^{-2} and ca. 25% Nafion® by mass from an ink consisting of Pd/C, Nafion solution and 1-propanol.

2.2. Electrochemistry

All electrochemical measurements were made in the 2-electrode flow-through cell shown schematically in Fig. 1A. It consists of a stainless steel body with stainless steel tubing and silicone gaskets to align and separate the two electrodes. The aqueous electrolyte solution (N_2-purged 0.1 mol dm^{-3} H_2SO_4 or 0.1 M formic acid in 0.1 mol dm^{-3} H_2SO_4) was pumped through the cell by a syringe pump (New Era Pump Systems Inc.), and all measurements were carried at ambient temperature (20±2 °C). Measurements were made with a model 273A EG&G Princeton Applied Research potentiostat/galvanostat controlled by CorrWare (Scribner), with the reference and counter electrode leads both connected to the downstream electrode. Cell resistances were measured at the open circuit potential by impedance spectroscopy using an EG&G Model 5210 Lock-in Amplifier and PowerSuite (EG&G) software. The almost constant real impedance at ca. 1000 Hz, which corresponded to a minimum in the imaginary impedance, was used.

In order to minimize the effects of the charging current, and to obtain currents at close to steady-state, staircase voltammetry with a 10 s step time, and 25 mV step height was employed. Reversal of the cell polarity was avoided by starting each scan at the open circuit potential. The

current at the end of each step was used to produce voltammograms and for analysis of the flow rate dependence of the current, following subtraction of the background current measured in 0.1 mol dm^{-3} H_2SO_4. In these measurement, the upstream electrode was always the anode, and the downstream Pt black electrode was the cathode, producing H_2. Consequently all potentials are referenced to DHE.

3. Results and discussion

3.1. Measurement of the cathode overpotential

One of the key features of the flow cell employed in this work was the absence of a dedicated reference electrode. Instead, the downstream cathode was expected to provide a stable reference potential during steady state measurements of anodic currents at the upstream working electrode. The validity of this assumption was examined by generating H_2 at both electrodes at zero flow rate. First, the potential was swept linearly from 0.0 V to 1 V to produce hydrogen at the downstream electrode. Then the polarity was reversed to -0.1 V to produce H_2 at the upstream electrode. The potential of the upstream electrode was then scanned between -0.02 and 0.11 V vs the downstream electrode at 1 mV s^{-1}. The resulting cyclic voltammogram (Fig. 2) showed a linear dependence of the current on potential, with a slope of ca. 18 Ω that was close to the cell resistance of ca. 17 Ω determined by impedance spectroscopy. Both the shape of the current (*I*) vs. potential (*E*) response, and the good agreement of the resistances, demonstrate that the overpotential was negligible for both H_2 oxidation and H^+ reduction.

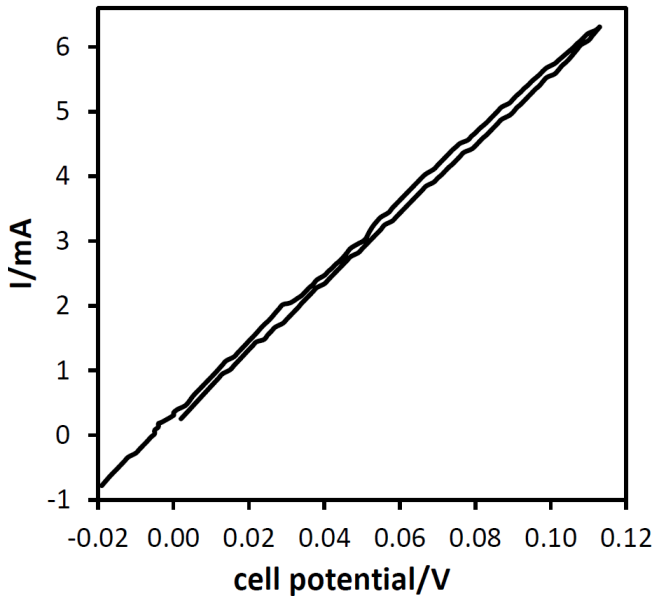

Figure 2. Cyclic voltammogram (1 mV s^{-1}) of a stationary 0.1 mol dm^{-3} ethanol in 0.1 mol dm^{-3} H_2SO_4(aq) solution in the flow-through cell following H_2 generation at both electrodes as described in the text.

3.2. Electrolysis of formic acid at Pd/C

Since Pd is much more active for formic acid oxidation than Pt, an electrode prepared with a commercial 40% Pd/C catalyst on a CFP support was used to characterize the hydrodynamic behavior of the cell. Fig. 3 shows the current vs. time response measured in a typical staircase voltammetry experiment. It can be seen that the rate of current decay at the end of each 10 s potential step was quite low. This step time allows data to be collected over a range of flow rates within a reasonable time period, and provides a compromise between allowing the background to decay and minimizing errors due to slow poisoning of the catalyst by CO [21]. A correction for the residual background current was made by subtracting the current at each potential and flow rate measured in the absence of formic acid. In addition, because of the large current passed in these experiments, a correction was also made for the cell resistance measured by impedance

spectroscopy. Fig. 4 shows the resulting voltammograms obtained over a range of flow rates between 0.05 and 0.3 cm^3 min^{-1}.

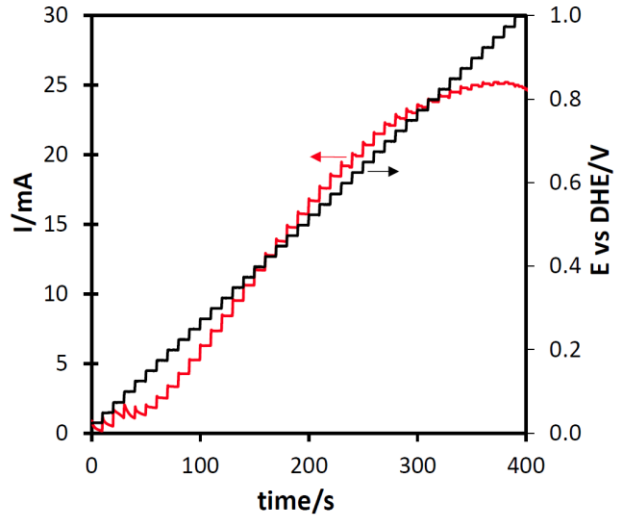

Figure 3. Current vs. time recorded during staircase voltammetry of 0.1 mol dm^{-3} formic acid in 0.1 mol dm^{-3} H_2SO_4(aq) at a Pd/C electrode, at 0.20 cm^3 min^{-1}.

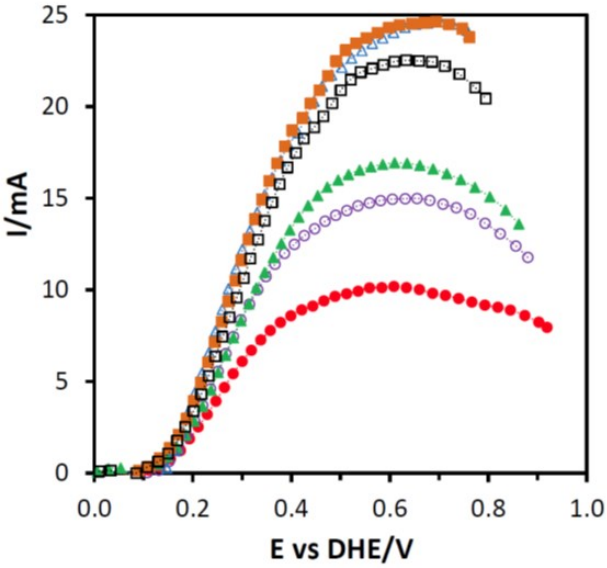

Figure 4. Background and resistance corrected staircase voltammograms for oxidation of 0.1 mol dm^{-3} formic acid in 0.1 mol dm^{-3} H_2SO_4(aq) at a Pd/C electrode, at flow rates of 0.05 (●), 0.10 (○), 0.15 (▲), 0.20 (△), 0.25 (■) and 0.30 (□) cm^3 min^{-1}.

The voltammograms in Fig. 4 show a strong dependence of the current on flow rate, although there are some anomalies in the flow rate dependence at high flow rates. This is most likely due to the formation of CO_2 bubbles within the catalyst layer, since at ca. 0.65 V, 23% to 63% of the formic acid entering the catalyst layer was being oxidized to CO_2. There are also anomalies in the 0 to 0.15 V range that can be attributed to inaccuracies in the background correction. There were larger background currents in this region due to desorption of H atoms from the catalyst surface.

The voltammograms in Fig. 4 show a broad peak at ca. 0.6 to 0.7 V due to the combination of the increasing rate of electron transfer, limitation of the current by the mass transport rate, and finally a decrease in the electron transfer rate at potential above ca. 0.65 V due to oxide formation on the Pd surface. There appears to be a mass transport limited plateau at the highest flow rates, but not at lower flow rates where it is presumably obscured by the peak in the electron transfer rate. In order to test for limitation of the current by mass transport, data from 0.5 to 0.6 V were analyzed by using eq. 1 [22]:

$$I = nFCu\,[1 - \exp(-\beta u^{\alpha-1})] \qquad (1)$$

Where C is the concentration of formic acid, u is the flow rate ($cm^3\ s^{-1}$), β is a constant determined by the mass transport and catalyst layer properties, and α is determined by the flow geometry. Eq. 1 accounts for the decrease in concentration of the formic acid as it passes through the catalyst layer, and the effect of the flow rate on the diffusion of formic acid to the catalyst particles. α is typically 0.33 to 0.5 for laminar flow [22]. Fig. 5 shows the data at 0.60 V from Fig. 4 as a function of flow rate, together with the best non-linear least squares fit to eq. 1. The best fit was obtained with $\alpha = 0.37$ at this potential and an average of $\alpha = 0.36 \pm 0.01$ was obtained for analysis of data

from 0.5 to 0.6 V. The almost constant value of α over this range suggests that the current was close to the mass transport limit.

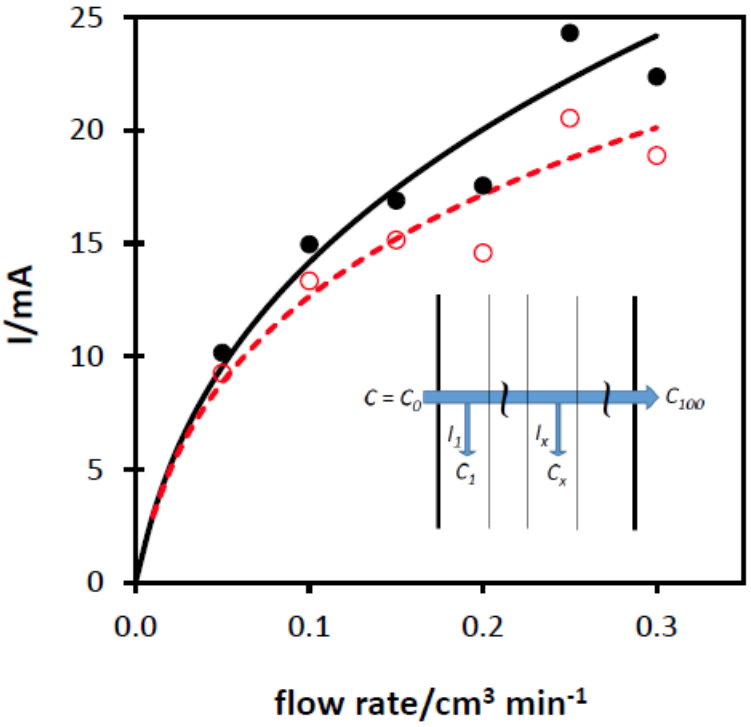

Figure 5. Current vs. flow rate for the oxidation of 0.1 mol dm^{-3} formic acid in 0.1 mol dm^{-3} H_2SO_4(aq) at a Pd/C electrode at 0.60 V (●) and 0.45 V (○), with best fit theoretical curves from eq. 1 (—), and eq. 2 (- - -) with λ = 217 mA s^{α} $cm^{3(1-\alpha)}$ mol^{-1} and α = 0.37. The inset shows a schematic diagram of the finite difference method used to simulate equation 2.

At lower potentials, when the current was below the mass transport limit, the kinetics of electron transfer must be taken into account in the analysis of the flow rate dependence of the current. Here we use a simplified version of a model reported by Alkire and Gracon [23]. The inset of Fig. 5 illustrates the finite difference method used to solve the model equations. The current at

each flow rate was calculated by dividing the thickness of the anode catalyst layer into 100 discrete layers in which the local current (I_x) is given by eq. 2:

$$C_{x-1}/100I_x = \frac{1}{n\lambda u^{\alpha}} + \frac{1}{nFk} \qquad (2)$$

where $n\lambda C_{x-1}u^{\alpha}$ is the mass transport limited current and $nFkC_{x-1}$ is the kinetic current in layer x. The rate constant (k), which has units of $cm^3\ s^{-1}$, applies to the whole catalyst layer, and can be used to calculate the kinetic current for the electrode (I_k), in the absence of local concentration polarization and changes in concentration with x, by using eq. 3.

$$I_k = nFkC \qquad (3)$$

It can be used to provide the heterogeneous rate constant for the catalyst ($cm\ s^{-1}$) by dividing by the electrochemically active area of the electrode (A_s). It is assumed in this model that there is a linear (steady-state) concentration gradient, perpendicular to the flow direction, between the concentration at the Pd surface and the concentration at the center of each pore [23].

The relationship expressed in eq. 2 between the current, kinetic current and mass transport limited current has been used to analyze steady state currents for formic acid [9], methanol [7], and ethanol [8] oxidation by RDV, and methanol and ethanol oxidation in a proton exchange membrane flow cell [24]. The change in concentration in each segment is given by eq. 4:

$$\Delta C_x = I_x/nFu \qquad (4)$$

The calculated total current (I) at each flow rate is the sum over all segments given by eq. 5.

$$I = \sum_{x=1}^{x=100} I_x \qquad (5)$$

For $I_k >> I$, this simulation reproduces the behaviour of eq. 1. In this model, it is assumed that the electrochemical kinetics are first order, and that the resistance of the catalyst layer is negligible.

Eq. 2 was first tested over the 0.5 to 0.6 V range, where fitting to eq. 1 suggested that the current was close to the mass transport limit. Good fits were obtained by allowing all three fitting

parameters (λ, α, k) to vary. The best fit values of α over this range were the same as those obtained by fitting the data to eq. 1, while the kinetic currents were all greater than 10 A, indicating that the current was at, or close to, the mass transport limit (i.e. the effect of the electron transfer rate was too small to significantly influence the flow rate dependence of the current).

Since λ and α should not vary with potential, they were set at the values of 217 mA s^{α} $cm^{3(1-\alpha)}$ mol^{-1} and 0.37, respectively, obtained at 0.6 V, for fitting the data at lower potentials. Although it was only necessary to fix one of these parameters to obtain acceptable fits and parameters, fixing both should provide more accurate kinetic parameters. Fig. 5 shows the best fit of eq. 2 to the data at 0.45 V from Fig. 4. Here the current was below the mass transport limit, and so under mixed kinetic-mass transport control.

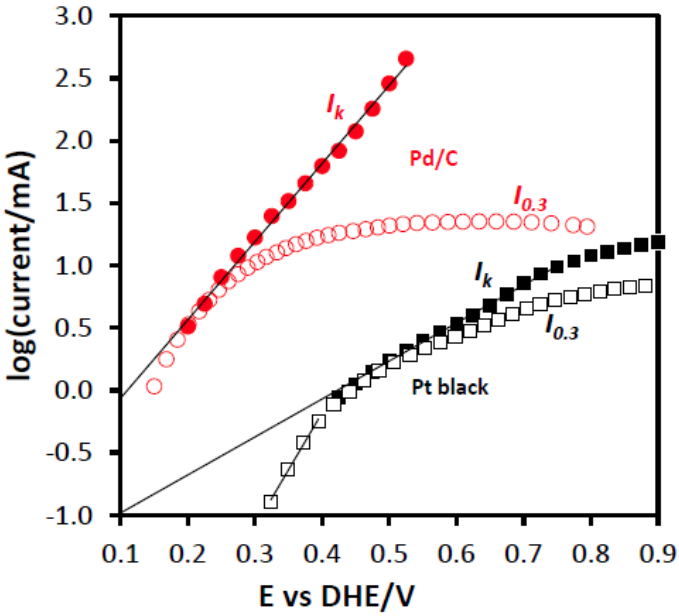

Figure 6. Tafel plots for the oxidation of 0.1 mol dm^{-3} formic acid in 0.1 mol dm^{-3} H_2SO_4(aq) at Pd/C (○, ●) and Pt black (□, ■) electrodes, showing the current measured at 0.3 cm^3 min^{-1} ($I_{0.3}$; ○, □), and the kinetic current (I_k; ●, ■) obtained by fitting the current vs. flow rate data in Figs. 4 and 7 to eq. 2.

Fig. 6 shows Tafel plots of I_k (from eq. 3) obtained by fitting the data in Fig. 4 to eq. 2, together with a Tafel plot of the experimental current at 0.3 cm^3 min^{-1} ($I_{0.3}$). The linearity of the log(I_k) plot and its convergence with the experimental current at low potentials both indicate that accurate separation of the effects of mass transport and electron transfer kinetics was achieved. It is also clear that the experimental current at 0.6 V was mass transport controlled, since I_k was much greater than $I_{0.3}$. The Tafel slope for I_k in Fig. 6 is 160 mV which is close to values previously reported for carbon supported Pd [25, 26]. The experimental currents at potentials below 0.2 V suggest that the Tafel slope may be lower at low potentials, but there is too much uncertainly to consider this to be significant.

The convergence of the kinetic and measured currents at ca. 0.2 V in Fig. 6 indicates that the effects of mass transport and the concentration change as the electrolyte solution flows through the electrode both become negligible. At higher potentials, the measured currents are not representative of the electron transfer rate, while at lower potentials a mass transport correction is not required (and becomes too inaccurate to be useful). The value of the methodology reported here is clearly seen at potentials above 0.2 V where it provides kinetic data in the mixed kinetic-mass transport region that is of most significance in electrocatalytic applications (fuel cells, electrolysis, etc.). It is notable that current densities of over 0.1 A cm^{-2} were achieved in these experiments for the oxidation of 0.1 mol dm^{-3} formic acid to H_2 and CO_2. The co-facial flow-through design of the cell may therefore have significance potential for large scale electrolysis of formic acid to produce H_2 at low cell potentials [3, 27].

Although separation of kinetic and mass transport influences on formic acid oxidation can also be conveniently accomplished by rotating disc voltammetry [9], it provides an apparent

kinetic current that includes an electron transfer component (I_e) coupled with a component due to diffusion of the reactant through the catalytic layer (I_s) according to eq. 6 [28].

$$I_k = (I_s I_e)^{1/2} \tanh(I_e/I_s)^{1/2} \qquad (6)$$

Consequently, the I_k values obtained depend on the permeability of the catalyst layer and it is very difficult to obtain the true heterogeneous rate constant for the catalyst (k/A_s) [29]. In contrast, use of a flow-through cell configuration and eq. 2 accounts for both the change in concentration as the reaction solution passes through the catalyst layer, and diffusion to the catalyst particles, and provides k directly. This provides a powerful method for comparing catalysts with minimal influence from the characteristics of the catalyst layer.

3.3. Electrolysis of formic acid at Pt black

Since formic acid oxidation is much slower at Pt than Pd, changing the working electrode to Pt black provided a test of eq. under conditions where the mass transport limited could not be reached, which is the normal situation for methanol and ethanol oxidation [7, 8]. Furthermore, use of a different type of catalyst structure (Pt black vs. carbon supported Pd) and binder (PTFE vs. Nafion), provides some insight into the effects of electrode structure on the mass transport parameters.

Fig. 7 shows background and resistance corrected staircase voltammograms at various flow rates for formic acid oxidation at a Pt black electrode. The currents were much lower than at the Pd/C electrode under the same conditions (Fig. 4), and consequently there was a much smaller dependence on flow rate. Also, there were no anomalies in the flow rate dependence at potentials above 0.7 V, suggesting that the anomalous behavior seen for Pd/C in Fig. 4 was due to the high amounts of CO_2 being produced. At lower potentials, the anomalies in the Pt black data can be attributed mainly to inaccuracy of the background correction.

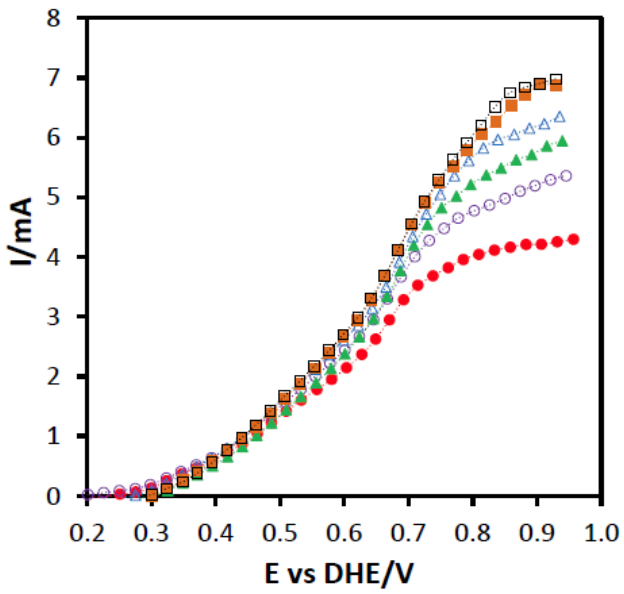

Figure 7. Background and resistance corrected staircase voltammograms for oxidation of 0.1 mol dm^{-3} formic acid in 0.1 mol dm^{-3} H_2SO_4(aq) at a Pt black electrode, at flow rates of 0.05 (●), 0.10 (○), 0.15 (▲), 0.20 (△), 0.25 (■) and 0.30 (□) cm^3 min^{-1}.

Since the currents at the Pt black electrode were much too low to be purely mass transport limited, the flow rate dependence was fitted by using eq. 2. It was assumed that α would be the same as for the Pd/C electrode ($\alpha = 0.37$), since the flow and electrode geometries were the same. Initially, the data from Fig. 7 were fitted to eq. 2 by varying both λ and k. The best fit values of k increased monotonically with increasing potential, while λ ranged between 92 and 153 mA s^{α} $cm^{3(1-\alpha)}$ mol^{-1}. Since λ determines the mass transport current, it should not vary with potential, and its accuracy should increase with increasing current, as the first term in eq. 2 becomes more significant. Consequently, λ was almost constant from 0.850 to 0.925 V, and the average value of 106±1 mA s^{α} $cm^{3(1-\alpha)}$ mol^{-1} over this range was used to refine the fits to eq. 2, to obtain more accurate values of k. Figure 8 shows examples of the fits to eq. 2, while Tafel plots of I_k (from eq.

3) and the experimental current at 0.3 cm^3 min^{-1} are included in Fig. 6. The Tafel slope obtained for the Pt black electrode was 109 mV in the kinetic region from ca. 0.3-0.4 V, but increased to 392 mV in the mixed kinetic/mass transport region from ca. 0.4 to 0.7 V. Zhao et al. [30] have reported a similar Tafel slope of ca. 95 mV in the kinetic region for oxidation of 0.1 mol dm^{-3} formic acid in 0.1 mol dm^{-3} H_2SO_4(aq) at Pt black from 0.25 to 0.4 V vs. RHE over timescales from 1 to 120 min. However, we are not aware of other kinetic data at higher potentials, which are most relevant to applications in fuel and electrolysis cells.

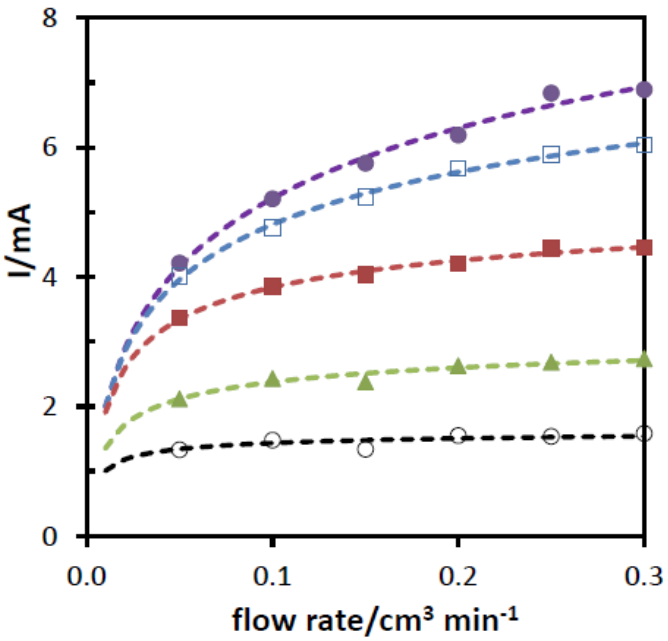

8. Current vs. flow rate for the oxidation of 0.1 mol dm^{-3} formic acid in 0.1 mol dm^{-3} H_2SO_4(aq) at 0.9 (●) 0.8 (◆), 0.7 (■), 0.6 (▲) and 0.5 (○) V, at a Pt black electrode, with best fit theoretical curves from eq. 2 (- - -) with λ = 106 mA s^{α} $cm^{3(1-\alpha)}$ mol^{-1} and α = 0.37.

Comparison of the kinetic currents for formic acid at Pd/C and Pt black in Fig. 6 reveals the very large, and well known [31, 32], intrinsic differences in the kinetics at these two metals. This is due to both a higher exchange current at Pd and a lower Tafel slope at currents above ca. 1

mA in Fig. 6. However, a quantitative comparison cannot be made here because the active areas of the electrodes are not known. The higher λ obtained for the Pd/C electrode suggests that its active area was approximately double that of the Pt black electrode, although the structure and porosity of the electrode also play a role in determining λ. Active areas can be determined by cyclic voltammetry (hydrogen adsorption and desorption), if a reference electrode is inserted between the two electrodes. However, the increased solution resistance can then make it difficult to determine λ.

The two electrode cell employed here has been designed primarily for the study of methanol and ethanol oxidation, where there are multiple products, and the number of electrons transferred (n) is unknown and variable. By calibrating the mass transport characteristics of each electrode with formic acid (n = 2), it may be possible to determine n values electrochemically for methanol and ethanol by using eq. 2. In addition, quantitative collection of products for analysis is straightforward and can be used to determine n for analysis of the kinetics with eq. 2.

4. Conclusions

The flow-through cell configuration employed here has many advantages over rotating disc voltammetry and other flow cell configurations for analysis of the kinetics of formic acid oxidation at fuel cell catalysts. It can be used with the same electrodes that are used in fuel cells, and provides higher utilization of the catalyst. By exposing the whole catalyst layer to the formic acid solution (Fig. 1C), and accounting for the decrease in concentration as it flows through the electrode, the true electron transfer rate constant is obtained, rather than an apparent kinetic current that contains a component due to diffusion of formic acid into the catalyst layer. Eq. 2 provides a powerful method for modelling the oxidation of formic acid in flow-through electrodes and quantitatively comparing different catalysts and structures. The cell and methodology reported here will be

particularly useful for unraveling the multiple processes and pathways in the oxidation of more complex fuels such as methanol and ethanol.

Acknowledgements

This work was supported by the Natural Sciences and Engineering Research Council of Canada [grant number 2017-04260] and Memorial University.

References

[1] B.C. Ong, S.K. Kamarudin, S. Basri, Direct liquid fuel cells: A review, International Journal of Hydrogen Energy, 42 (2017) 10142-10157.

[2] C. Coutanceau, S. Baranton, Electrochemical conversion of alcohols for hydrogen production: a short overview, Wiley Interdisciplinary Reviews-Energy and Environment, 5 (2016) 388-400.

[3] E.O. Kilic, A.S. Koparal, U.B. Ogutveren, Hydrogen production by electrochemical decomposition of formic acid via solid polymer electrolyte, Fuel Processing Technology, 90 (2009) 158-163.

[4] Y.Z. Zhao, X.M. Li, J.M. Schechter, Y.A. Yang, Revisiting the oxidation peak in the cathodic scan of the cyclic voltammogram of alcohol oxidation on noble metal electrodes, RSC Advances, 6 (2016) 5384-5390.

[5] P. Hernandez-Fernandez, P.B. Lund, C. Kallesoe, H.F. Clausen, L.H. Christensen, Supported Pt-based nanoparticulate catalysts for the electro-oxidation of methanol: An experimental protocol for quantifying its activity, International Journal of Hydrogen Energy, 40 (2015) 284-291.

[6] A. Boronat-Gonzalez, E. Herrero, J.M. Feliu, Fundamental aspects of HCOOH oxidation at platinum single crystal surfaces with basal orientations and modified by irreversibly adsorbed adatoms, Journal of Solid State Electrochemistry, 18 (2014) 1181-1193.

[7] A. Sayadi, P.G. Pickup, Evaluation of methanol oxidation catalysts by rotating disc voltammetry, Electrochimica Acta, 199 (2016) 12-17.

[8] A. Sayadi, P.G. Pickup, Evaluation of ethanol oxidation catalysts by rotating disc voltammetry, Electrochimica Acta, 215 (2016) 84-92.

[9] A. Sayadi, P.G. Pickup, Electrochemical oxidation of formic acid at carbon supported Pt coated rotating disk electrodes, Russian Journal of Electrochemistry, 53 (2017) 1054-1060.

[10] R. Zhou, Y. Zheng, M. Jaroniec, S.-Z. Qiao, Determination of the electron transfer number for the oxygen reduction reaction: From theory to experiment, ACS Catalysis, 6 (2016) 4720-4728.

[11] D. Pletcher, R.A. Green, R.C.D. Brown, Flow Electrolysis Cells for the Synthetic Organic Chemistry Laboratory, Chemical Reviews, 118 (2018) 4573-4591.

[12] D.M. Weekes, D.A. Salvatore, A. Reyes, A.X. Huang, C.P. Berlinguette, Electrolytic CO_2 Reduction in a Flow Cell, Accounts of Chemical Research, 51 (2018) 910-918.

[13] T. Noyhouzer, S.C. Perry, A. Vicente-Luis, P.L. Hayes, J. Mauzeroll, The Best of Both Worlds: Combining Ultramicroelectrode and Flow Cell Technologies, Journal of the Electrochemical Society, 165 (2018) H10-H15.

[14] G. Muthuraman, L. Boyeol, M. Il-Shik, Na-beta-Alumina as a Separator in the Development of All-Vanadium Non-Aqueous Tubular Redox Flow Batteries: An Electrochemical and Charging-Discharging Examination Using a Prototype Tubular Redox Flow Cell, Journal of the Electrochemical Society, 165 (2018) A1920-A1924.

[15] S.E. Temmel, S.A. Tschupp, T.J. Schmidt, A highly flexible electrochemical flow cell designed for the use of model electrode materials on non-conventional substrates, Review of Scientific Instruments, 87 (2016) 045115.

[16] Z. Jusys, J. Kaiser, R.J. Behm, A novel dual thin-layer flow cell double-disk electrode design for kinetic studies on supported catalysts under controlled mass-transport conditions, Electrochimica Acta, 49 (2004) 1297-1305.

[17] S. Sun, M.C. Halseid, M. Heinen, Z. Jusys, R.J. Behm, Ethanol electrooxidation on a carbon-supported Pt catalyst at elevated temperature and pressure: A high-temperature/high-pressure DEMS study, Journal of Power Sources, 190 (2009) 2-13.

[18] G.C. Luque, M.R.G. de Chialvo, A.C. Chialvo, Kinetic Study of the Formic Acid Oxidation on Steady State Using a Flow Cell, Journal of the Electrochemical Society, 64 (2017) H748-H754.

[19] X.M. Ren, T.E. Springer, T.A. Zawodzinski, S. Gottesfeld, Methanol transport through Nafion membranes - Electro-osmotic drag effects on potential step measurements, Journal of the Electrochemical Society, 147 (2000) 466-474.

[20] X. Ren, T.E. Springer, S. Gottesfeld, Water and methanol uptakes in Nafion membranes and membrane effects on direct methanol cell performance, Journal of the Electrochemical Society, 147 (2000) 92-98.

[21] X. Yu, P.G. Pickup, Mechanistic study of the deactivation of carbon supported Pd during formic acid oxidation, Electrochemistry Communications, 11 (2009) 2012-2014.

[22] A.J. Bard, L.R. Faulkner, Electrochemical methods. Fundamentals and applications, 2 nd ed., Wiley, New York, 2001.

[23] R. Alkire, B. Gracon, Flow-through porous-electrodes, Journal of the Electrochemical Society, 122 (1975) 1594-1601.

[24] T.M. Brueckner, P.G. Pickup, Kinetics and stoichiometry of methanol and ethanol oxidation in multi-anode proton exchange membrane cells, Journal of the Electrochemical Society, 64 (2017) F1172-F1178.

[25] Y. Liu, L.W. Wang, G. Wang, C. Deng, B. Wu, Y. Gao, High active carbon supported PdAu catalyst for formic acid electrooxidation and study of the kinetics, Journal of Physical Chemistry C, 114 (2010) 21417-21422.

[26] M. Rezaei, S.H. Tabaian, D.F. Haghshenas, The role of electrodeposited Pd catalyst loading on the mechanisms of formic acid electro-oxidation, Electrocatalysis, 5 (2014) 193-203.

[27] C. Lamy, A. Devadas, M. Simoes, C. Coutanceau, Clean hydrogen generation through the electrocatalytic oxidation of formic acid in a proton exchange membrane electrolysis cell (PEMEC), Electrochimica Acta, 60 (2012) 112-120.

[28] S. Amarasinghe, T.Y. Chen, P. Moberg, H.J. Paul, F. Tinoco, L.A. Zook, J. Leddy, Models for mediated reactions at film-modified electrodes - controlled electrode potential, Analytica Chimica Acta, 307 (1995) 227-244.

[29] F. Gloaguen, F. Andolfatto, R. Durand, P. Ozil, Kinetic-study of electrochemical reactions at catalyst-recast ionomer interfaces from thin active layer modeling, Journal of Applied Electrochemistry, 24 (1994) 863-869.

[30] M.C. Zhao, C. Rice, R.I. Masel, P. Waszczuk, A. Wieckowski, Kinetic study of electro-oxidation of formic acid on spontaneously-deposited Pt/Pd nanoparticles - CO tolerant fuel cell chemistry, Journal of the Electrochemical Society, 151 (2004) A131-A136.

[31] K. Jiang, H.X. Zhang, S.Z. Zou, W.B. Cai, Electrocatalysis of formic acid on palladium and platinum surfaces: from fundamental mechanisms to fuel cell applications, Physical Chemistry Chemical Physics, 16 (2014) 20360-20376.

[32] H. Jeon, B. Jeong, J. Joo, J. Lee, Electrocatalytic oxidation of formic acid: Closing the gap between fundamental study and technical applications, Electrocatalysis, 6 (2015) 20-32.